Phosphorus/reduced graphene oxide nanocomposite for high-performance anode of sodium-ion batteries

Meng Li,[1§] Su Dou,[1,2§] Na Feng,[1] Xiong Pu,[1*] Weiguo Hu[1*]

[1]*Beijing Institute of Nanoenergy and Nanosystems, Chinese Academy of Sciences, Beijing 100083, China*
[2]*School of Materials Science and Engineering, University of Science and Technology Beijing, Beijing 100083, China*
[§] *These authors contributed equally to this work.*

[*]Corresponding author

DOI: 10.5185/amlett.2018.1871
www.vbripress.com/aml

Abstract

The red phosphorus is considered as a promising anode material for sodium-ion batteries (SIBs) due to its high theoretical capacity of 2596 mAh/g. However, red phosphorus suffers from some limitations, such as low electronic conductivity, and huge volume expansion in the process of discharging. Herein, we report a high-performance anode with red phosphorus (rP)/reduced graghene oxide (rGO) nanocomposite *via* vaporization-condensation method. The resulting nanostructured rP is uniformly distributed on the surfaces of rGO. The obtained rP/rGO anode achieves high reversibility (76.85% initial columbic efficiency), high specific discharge capacity (1582.3 mAh/g at 260 mA/g), stable cycling performances (60.2% capacity retention after 50 cycles), and high rate performances (up to 7800 mA/g current density). These high performances of our nanocomposite materials suggest that the rP/rGO anode is of great potential for future high energy SIBs.
Copyright © 2018 VBRI Press.

Keywords: Reduced graphene oxide, red phosphorus, sodium ion batteries.

Introduction

In terms of energy storage, lithium-ion batteries (LIBs) have dominated the portable electronic devices market for decades owing to their high energy density and stable cycling behavior.[1-3] However there are some limits about the use of LIBs due to the looming cost and resource depletion. Sodium-ion batteries(SIBs) are the attractive alternatives to LIBs[4-6], due to the abundant resources and potentially lower price. Among various anode materials, red phosphorus (rP) possesses the highest specific capacity of 2596 mAh/g because of the formation of Na_3P[7-12]. However, there are still some concerns about the SIBs with regards to the cycling life and rate performance because of its poor electrical performance, large volume change (about 400%) and pulverization of red phosphorus particles[13-16]. Thus considerable efforts have been dedicated to designing the novel and composite anode materials between P and conduct carbon-based materials[17, 18]. For example, Qian *et al.* reported firstly the amorphous phosphorus/ carbon nanocomposite *via* facile high energy ball-milling process, which delivered a high reversible capacity of 1750 mAh/g after 40 cycles at a current density of 250 mA/g[19]. Similarly, Kim *et al.* demonstrated that the amorphous red phosphorus/carbon hybrids prepared by ball milling showed a high capacity of 1890 mAh/g at current density of 143 mA/g and less than 7% capacity fading after 30 cycles[20]. Chou *et al.* synthesized a anode composite by hand-grinding commercial microsized red phosphorus and carbon nanotubes, achieving a high reversible capacity of 1675mAh/g[21]. Despite these improvements, the cycling stability performance is still low. On the other hand, red phosphorus and carbon-based materials mixed by vaporization condensation method have attracted intensive attentions.[22-24]. This method was firstly introduced by Monconduit *et al*.[17] and He *et al*.[13] to fabricate a nanostructured red phosphorus composite, which could deliver a high reversible capacity and stable cycling.

Herein, we prepared rP/rGO composite *via* vaporization condensation method, where rGO is crucial as a mechanically supporting matrix to buffer the volume variation of rP and also as a conductive additive to overcome the poor electrical conductivity of rP. The final nanocomposite showed intimate contact between the rGO and rP. The rational combination of highly conductive rGO and high-capacity rP led to the excellent electrochemical performances of the nanocomposite anode, which achieved high reversibility (76.85% initial columbic efficiency), high specific discharge capacity (1582.3 mAh/g at 260 mA/g), stable cycling performances (60.2% capacity retention after 50 cycles), and high rate performances (up to 7800 mA/g current density).

Experimental

The synthesis of rP/rGO composite

Firstly, graphene oxide (GO) was prepared by the Hummer's method. The obtained GO was held at 1000 ℃ for 2 h in Ar atomsphere to prepare the rGO. **Fig. 1a** represents a schematic illustration of the synthesis procedures of rP/rGO composite *via* vaporization condensation method[23]. Typically, 0.1 g of rGO and 0.2 g of red phosphorus were placed in a sealed vacuum vessel. The sealed vacuum vessel was put in a furnace, which was raised to 500 ℃ at the rate of 4 ℃/min. and then held for 2 h. At his high temperature, red phosphorus was vaporized and infiltrated onto the surfaces of rGO. To avoid the formation of white P, the vessel was cooled to 260 ℃ at 1 ℃/min and held for 24 h. After the heat treatment process, the vessel was cooled to room temperature naturally, and the rP/rGO was obtained by washing with the produces with CS_2 to remove the residual white P and then drying under vacuum. The temperature profiles of the whole process are showed in **Fig. 1b**.

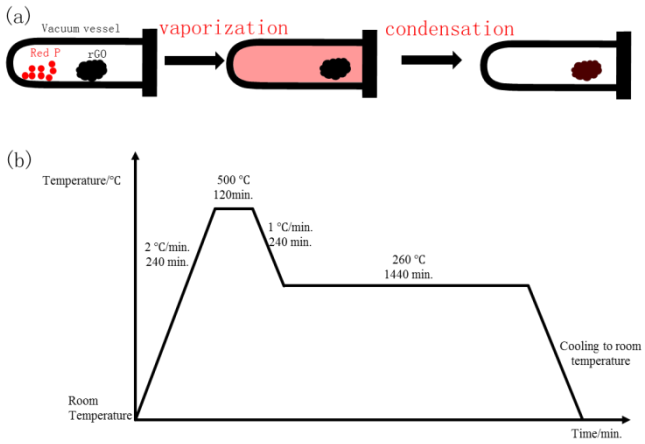

Fig. 1. (a) Schematic illustration of rP/rGO synthesis, and (b) schematic description of the temperature variation of vaporization condensation method.

Structure characterization

The morphology of the red phosphorus an rGO is characterized by a scanning electron microscope (Hitachi SU8020). A field emission transmission electron microscopy (FEI/Tecnai G2 F20) was employed to obtain the TEM images with EDS profiles. For preparing the TEM samples, rP/rGO nanocomposite was dispersed in ethanol and dropcast onto a Cu TEM grid.

Electrochemical characterization

Battery performance was conducted in CR2032 coin cells with sodium foil as counter electrode, rP/rGO electrode as the working electrode, and Whatman glass fiber separator. The electrolyte was 1 M $NaClO_4$ dissolved in ethylene carbonated (EC) and diethyl carbonated (DEC) (1:1 v/v) solution with 5% fluroethylene carbonated (FEC). The rP/rGO composite was mixed with carbon black (Super P) and Sodium polyacrylate (PAAS) in a 7:1:2 weight ratio. The electrode mixture were mixed in water, and coated on Cu foil with a doctor blade. All batteries were assembled in an argon-filled glove box with water and oxygen content below 0.1 ppm. The mass loading of the electrodes was about 1 mg/cm^2. The specific discharge capacity was calculated based on the weight of rP/rGO composite.

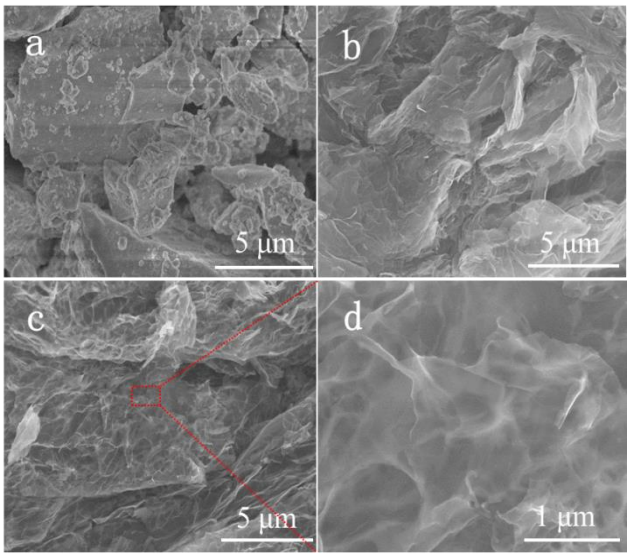

Fig. 2. (a) SEM images of pristine commercial phosphorus, (b) as-prepared rGO, and (c) rP/rGO composite. (d) The enlarged SEM image in the area marked with red rectangle in (c).

Results and discussion

Fig. 2a shows the SEM image of the commercial rP particles with the size of tens of micrometer. After reduction of GO, thin rGO flakes with micrometer scale size and nanometer scale thickness can be observed, as shown in **Fig. 2b**. According to our previous results, the reduction of GO at 1000 ℃ in Ar atmosphere can result in rGO with high conductivity and large specific surface area. Therefore, large amount of rP can be infiltrated on rGO, resulting in the high weight ratio of rP in the composite. In this study, the original P:C weight ratio in the vacuum vessel before heat treatment was 2:1. The SEM images of the rP/rGO nanocomposite are shown in **Fig. 2c** and **d**. No large rP particles or aggregates can be observed after the vaporization condensation method (**Fig. 2c**), confirming that the rP are conformably and uniformly deposited onto the surfaces of the rGO. Even with the rP coatings, the porous morphology of the nanocomposite can still be observed (see **Fig. 2d**). Energy Dispersive Spectrometer (EDS) mapping under Scanning Transmission Electron Microscopy (STEM) was also performed to further confirm the uniform distribution of rP on rGO, as shown by a rP/rGO flake in **Fig. 3a**. Both the two elements of Phosphorus (**Fig. 3b**) and Carbon (**Fig. 3c**) are evenly distributed on the rGO flake. The shape of the converged mapping of all two elements in **Fig. 3d** well accords with the image of the nanocomposited particles in **Fig. 3a**.

Copyright © 2018 VBRI Press

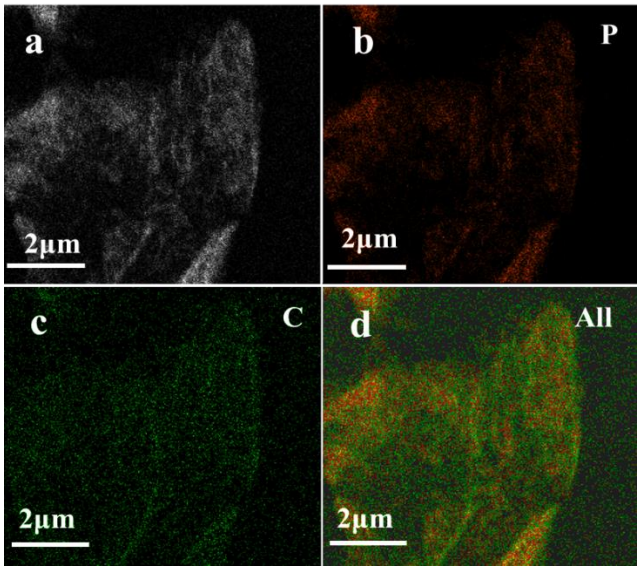

Fig.3. (a) a TEM image of rP/rGO composite, and corresponding elemental mapping images of (b) phosphorus, (c) carbon and (d) converged distribution of all elements.

The rP/rGO nanocomposite has following benefits: First, the size of the rP is significantly reduced comparing with original commercial rP, leading to the greatly shortened transfer paths for both sodium ions and electrons. Second, the specific surface area of the nanocomposite will also be greatly improved comparing with the commercial micoscale rp particles, due to the reduced particle size. Therefore, the active sites for redox actions during the charge/discharge cycles will be largely improved. Meanwhile, the porous structure of the nanocomposite can also facilitate the electrolyte infiltration and therefore improve the reaction kinetics. Third, the highly conductive rGO can function as abundant micro-electron-collectors, which *in situ* provide high rate paths for electrons flowing from (or to) the less conductive rP. As a result, the poor conductivity of the rP can be overcome. Last, the porous structure and nanosized morphology of the nanocomposite can alleviate the volume variation of the rP during the cycling. The micro-pores provide enough spaces for the volume expansion, and the intimate contact between the rGO and rP can ensure that rP layers will maintain the electrical contact and therefore not become "dead" sites during elongated cycling.

The cycling performances of rP/rGO nanocomposite and pure red phosphorus are compared by galvanostatic charge/discharge of the electrodes between 0.01 and 2 V *vs*. Na/Na^+ at a current density of 260 mA/g, as showed in **Fig. 4a**. The nanocomposite showed an initial specific discharge capacity of 1582.3 mAh/g, largely improved from the 984 mAh/g of the pure rP. It should be noted that the specific capacity of the nanocomposite is based on the total weight of rGO and rP. After 50 cycles, the nanocomposite maintains specific discharge capacity of 952.7 mAh/g at the 260 mA/g, correspondence to a capacity retention of 60.2%. In the contrast, the capacity of the commercial rP quickly drops to less than 100 mAh/g in 5 cycles. Furthermore, the nanocomposite shows 76.85% columbic efficiency for the first cycle, and the efficiencies of the following cycles are maintained to be more than 98%; while for the pure rP, the initial columbic efficiency is only 19.1%.

Based on these results, it is suggested that the pure rP showed low capacity and very low reversibility. The low capacity is mainly due to the low conductivity of the large rP particles, which cannot fully engage in the redox reactions with sodium ions for the first cycle. Meanwhile, the large volume change after the 1st will lead to the particle fracture and loss of electrical contact, making the pulverized rP inaccessible for further reactions.[25] In the contrast, the high discharge capacity of the nanocomposite indicates the high rate charge transfers in the cycling. The stable cycling performances and high reversibility of rP/rGO composite also confirm that the large volume expansion of the rP can be accommodated by the nanocomposite.

The charge-discharge profiles of the rP/rGO composite are depicted in **Fig. 4b** with cycle numbers labeled on individual curve. The small capacity difference between the first charge and discharge profiles is observed, which reveals that the irreversible capacity loss is small. Furthermore, three slopes located around 0.5, 0.7, and 1.4 V in the charge curves are observed, coinciding with the literature values[19].

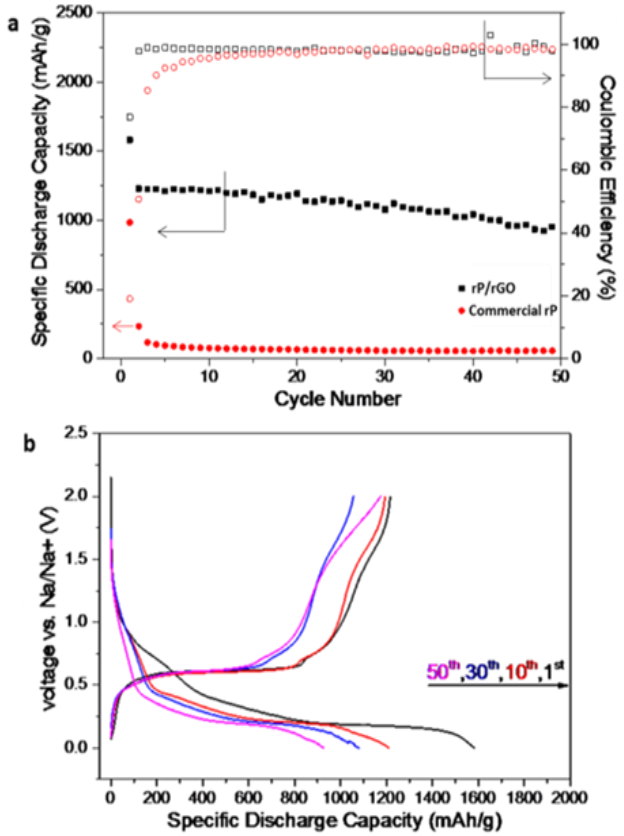

Fig. 4. (a) Cycling performance of the rP/rGO anode and commercial rP at a charge/discharge current density of 260 mA/g. (b) Corresponding potential profiles of the rP/rGO anode. The capacities here are calculated based on the total mass of rP/rGO composite.

Copyright © 2018 VBRI Press

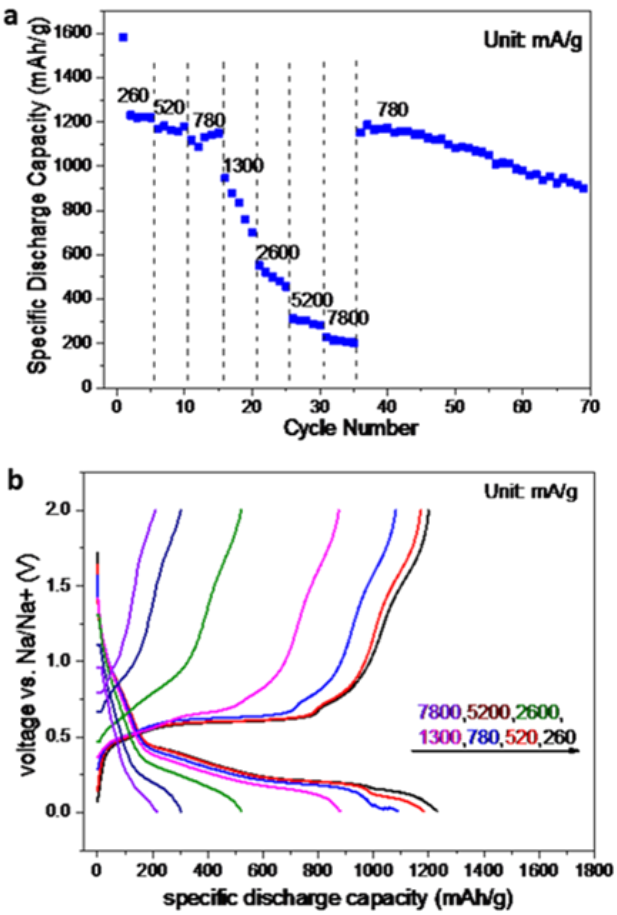

Fig. 5. (a) Rate performance of the rP/rGO anode with its potential profiles presented in (b). The capacities here are calculated based on the total mass of rP/rGO composite.

The rate capability of the rP/rGO nanocomposite at charge/discharge current densities ranging from 260 to 7800 mA/g is also evaluated, as shown in **Fig. 5a**. As increasing the current density, specific discharge capacity of 1207, ~1200, ~1100, ~800, ~500, ~300, and ~200 mAh/g are obtained at 260, 520, 780, 1300, 2600, 5200, and 7800 mA/g, respectively. Even at a high current rate of 7800 mA/g, the reversible capacity can still reach ~200 mAh/g. In addition, the capacity increase back to ~1100 mAh/g after decreasing the current density to 780 mA/g at 36th cycle, close to the capacity values of the initial 780mA/g test. Meanwhile, after 34 cycles of charge/discharge at 780 mA/g, the retained capacity is 898.5 mAh/g, further confirming the great cycling performances of the rP/rGO nanocomposite. **Fig. 5b** presents the charge-discharge voltage profiles of the rP/rGO anode at different current densities. The enlarged hysteresis is observed with the increasing of current densities. Similar to the previous reports, major sodiation and desodiation potential windows at 0.2-0.1 V and 0.6-0.7 V, respectively, is observed for the rP/rGO composite at low current density below 2600 mA/g. The plateau is implicit and the composite is presenting a potential curves similar to the supercapacitor at high current density of 7800 mA/g. However, the potential plateau of the composite is visible at 5200 mA/g. Thus the rate performance of the rP/rGO anode is greatly improved because of nanosized phosphorus and the outstanding electrical conductivity provided by the rGO.

Conclusion

In summary, we presented a rP/rGO nanocomposite for anode materials in SIBs. With the aid of vaporization condensation method, nanosized red phosphorus was uniformly coated onto the rGO flakes. The highly conductive rGO provided paths for high-rate charge transfers, and enough void spaces for accommodating the volume expansions of rP during cycling. Therefore, comparing with the low reversibility and short cycling life of commercial large size rP particles, the obtained rP/rGO nanocomposite achieved a specific discharge capacity of 952.7 mAh/g even after 50 cycles at the charge-discharge current density of 260 mA/g and an excellent rate capability at different current densities. The rational design of rP-based nanocomposite presented in this study has been demonstrated to be an effective approach for high energy density anode materials of future SIBs.

Acknowledgements

The authors thank for the support from National Natural Science Foundation of China (Grant Nos. 61574018 and 51603013), the Youth Innovation Promotion Association of Chinese Academy of Sciences, "Hundred Talents Program" of the Chinese Academy of Sciences, and National Key Research and Development Program of China (2016YFA0202703).

References

1. P.G. Bruce, B. Scrosati, J.-M. Tarascon, Nanomaterials for Rechargeable Lithium Batteries, Angewandte Chemie International Edition, *47* **(2008)** *2930-2946*.
2. U. Kasavajjula, C. Wang, A.J. Appleby, Nano- and bulk-silicon-based insertion anodes for lithium-ion secondary cells, Journal of Power Sources, *163* **(2007)** *1003-1039*.
3. A.S. Aricò, P. Bruce, B. Scrosati, J.-M. Tarascon, W. Van Schalkwijk, Nanostructured materials for advanced energy conversion and storage devices, Nature materials, *4* **(2005)** *366-377*.
4. B. Dunn, H. Kamath, J.-M. Tarascon, Electrical energy storage for the grid: a battery of choices, Science, *334* **(2011)** *928-935*.
5. W. Luo, F. Shen, C. Bommier, H. Zhu, X. Ji, L. Hu, Na-ion battery anodes: materials and electrochemistry, Accounts of chemical research, *49* **(2016)** *231-240*.
6. J. Ding, H. Wang, Z. Li, A. Kohandehghan, K. Cui, Z. Xu, B. Zahiri, X. Tan, E.M. Lotfabad, B.C. Olsen, Carbon nanosheet frameworks derived from peat moss as high performance sodium ion battery anodes, ACS nano, *7* **(2013)** *11004-11015*.
7. W.H. Ryu, H. Wilson, S. Sohn, J. Li, X. Tong, E. Shaulsky, J. Schroers, M. Elimelech, A.D. Taylor, Heterogeneous WSx/WO(3) Thorn-Bush Nanofiber Electrodes for Sodium-Ion Batteries, ACS nano, *10* **(2016)** *3257-3266*.
8. Y. Wang, J. Liu, B. Lee, R. Qiao, Z. Yang, S. Xu, X. Yu, L. Gu, Y.S. Hu, W. Yang, K. Kang, H. Li, X.Q. Yang, L. Chen, X. Huang, Ti-substituted tunnel-type Na(0).(4)(4)MnO(2) oxide as a negative electrode for aqueous sodium-ion batteries, Nature communications, *6* **(2015)** *6401*.
9. Y. Xie, Y. Dall'Agnese, M. Naguib, Y. Gogotsi, M.W. Barsoum, H.L. Zhuang, P.R. Kent, Prediction and characterization of MXene nanosheet anodes for non-lithium-ion batteries, ACS nano, *8* **(2014)** *9606-9615*.
10. C. Zhu, X. Mu, P.A. van Aken, Y. Yu, J. Maier, Single-layered ultrasmall nanoplates of MoS2 embedded in carbon nanofibers with excellent electrochemical performance for lithium and sodium

Copyright © 2018 VBRI Press

storage, Angewandte Chemie International Edition, *53* **(2014)** *2152-2156*.
11. H. Hou, C.E. Banks, M. Jing, Y. Zhang, X. Ji, Carbon Quantum Dots and Their Derivative 3D Porous Carbon Frameworks for Sodium-Ion Batteries with Ultralong Cycle Life, Advanced materials, *27* **(2015)** *7861-7866*.
12. W.S. Hummers Jr, R.E. Offeman, Preparation of graphitic oxide, Journal of the American Chemical Society, *80* **(1958)** *1339-1339*.
13. L. Wang, X. He, J. Li, W. Sun, J. Gao, J. Guo, C. Jiang, Nano-structured phosphorus composite as high-capacity anode materials for lithium batteries, Angewandte Chemie, *51* **(2012)** *9034-9037*.
14. J. Song, Z. Yu, M.L. Gordin, X. Li, H. Peng, D. Wang, Advanced sodium ion battery anode constructed via chemical bonding between phosphorus, carbon nanotube, and cross-linked polymer binder, ACS nano, *9* **(2015)** *11933-11941*.
15. Y. Zhu, Y. Wen, X. Fan, T. Gao, F. Han, C. Luo, S.-C. Liou, C. Wang, Red phosphorus–single-walled carbon nanotube composite as a superior anode for sodium ion batteries, ACS Nano, *9* **(2015)** *3254-3264*.
16. J. Sun, H.-W. Lee, M. Pasta, Y. Sun, W. Liu, Y. Li, H.R. Lee, N. Liu, Y. Cui, Carbothermic reduction synthesis of red phosphorus-filled 3D carbon material as a high-capacity anode for sodium ion batteries, Energy Storage Materials, *4* **(2016)** *130-136*.
17. C. Marino, A. Debenedetti, B. Fraisse, F. Favier, L. Monconduit, Activated-phosphorus as new electrode material for Li-ion batteries, Electrochemistry Communications, *13* **(2011)** *346-349*.
18. C. Marino, L. Boulet, P. Gaveau, B. Fraisse, L. Monconduit, Nanoconfined phosphorus in mesoporous carbon as an electrode for Li-ion batteries: performance and mechanism, Journal of Materials Chemistry, *22* **(2012)** *22713*.
19. J. Qian, X. Wu, Y. Cao, X. Ai, H. Yang, High capacity and rate capability of amorphous phosphorus for sodium ion batteries, Angewandte Chemie, *52* **(2013)** *4633-4636*.
20. Y. Kim, Y. Park, A. Choi, N.S. Choi, J. Kim, J. Lee, J.H. Ryu, S.M. Oh, K.T. Lee, An amorphous red phosphorus/carbon composite as a promising anode material for sodium ion batteries, Advanced materials, *25* **(2013)** *3045-3049*.
21. W.J. Li, S.L. Chou, J.Z. Wang, H.K. Liu, S.X. Dou, Simply mixed commercial red phosphorus and carbon nanotube composite with exceptionally reversible sodium-ion storage, Nano letters, *13* **(2013)** *5480-5484*.
22. W. Li, S. Hu, X. Luo, Z. Li, X. Sun, M. Li, F. Liu, Y. Yu, Confined Amorphous Red Phosphorus in MOF-Derived N-Doped Microporous Carbon as a Superior Anode for Sodium-Ion Battery, Advanced materials, *29* **(2017) 1605820**.
23. W. Li, Z. Yang, Y. Jiang, Z. Yu, L. Gu, Y. Yu, Crystalline red phosphorus incorporated with porous carbon nanofibers as flexible electrode for high performance lithium-ion batteries, Carbon, *78* **(2014)** *455-462*.
24. W. Li, Z. Yang, M. Li, Y. Jiang, X. Wei, X. Zhong, L. Gu, Y. Yu, Amorphous Red Phosphorus Embedded in Highly Ordered Mesoporous Carbon with Superior Lithium and Sodium Storage Capacity, Nano letters, *16* **(2016)** *1546-1553*.
25. H. Wu, G. Chan, J.W. Choi, I. Ryu, Y. Yao, M.T. McDowell, S.W. Lee, A. Jackson, Y. Yang, L. Hu, Y. Cui, Stable cycling of double-walled silicon nanotube battery anodes through solid-electrolyte interphase control, Nature nanotechnology, *7* **(2012)** *310-315*.

Copyright © 2018 VBRI Press